Mine Water Environ (2012) 31:273–286
DOI 10.1007/s10230-012-0199-z

TECHNICAL ARTICLE

Capacity of Wood Ash Filters to Remove Iron from Acid Mine Drainage: Assessment of Retention Mechanism

Thomas Genty · Bruno Bussière · Mostafa Benzaazoua · Gérald J. Zagury

Received: 5 December 2011 / Accepted: 1 August 2012 / Published online: 19 August 2012

Abstract Acid mine drainage (AMD) with high iron concentrations can be a major challenge for passive treatment systems, particularly when sulphate reducing passive bioreactors (SRPBs) are used. The capacity of wood ash filters to act as a polishing step after SRPB treatment of a high-iron AMD (4,000 mg L^{-1} of Fe) was assessed. Five columns (1.7 L) with different mixtures of wood combustion ash and sand were investigated for their potential to remove metals from an SRPB effluent over 122 days. These materials had a high specific surface area (between 46 and 159 m^2 g^{-1}), high organic carbon contents (between 12 and 32 %), and a high paste pH (up to 12.2). The Freundlich isotherm model reflects the observed iron sorption behavior on the material surface. Column study results indicate that the wood ash decreased iron concentrations for more than 100 days below 10 mg L^{-1} (99 % iron removal), mainly due to iron hydroxide precipitation and sorption. The risk of system clogging was negligible since the saturated hydraulic conductivity remained stable, between 5.0×10^{-3} and 3.1×10^{-2} cm s^{-1}. Between 44 and 52 % of the sulphate was also removed due to gypsum precipitation.

Keywords Column tests · Sorption · Passive treatment · Reuse of by-product

Introduction

Wastes produced during mining operations can significantly contaminate drainage water (Aubertin et al. 2002; Blowes and Ptacek 1994; Evangelou and Zhang 1995; Kleinmann et al. 1981). Several methods exist to treat acid mine drainage (AMD) and attain regulatory criteria; active lime treatment is the most commonly used.

At closed mine sites, passive treatment systems are preferred because they use natural or waste materials and have low operating and maintenance costs (Johnson and Hallberg 2005; Neculita et al. 2007; Skousen and Ziemkiewicz 2005). Passive treatment systems, such as anoxic limestone drains (ALDs) and sulfate-reducing passive biofilters (SRPBs), have demonstrated their effectiveness, at least in the short term, for slightly or moderately-contaminated AMD (Cravotta and Trahan 1999; Hedin et al. 1994). However, their capacity to treat highly contaminated AMD (especially with high iron concentrations) still has to be demonstrated (Genty et al. 2012). Costa et al. (2008), Neculita and Zagury (2008), and Potvin (2009) showed that SRPBs could effectively treat AMD with iron concentrations up to approximately 500 mg L^{-1}. Genty (2012) tested eight different SRPBs in batch and column tests to treat a high iron acid mine drainage (pH 3.5,

Electronic supplementary material The online version of this article (doi:10.1007/s10230-012-0199-z) contains supplementary material, which is available to authorized users.

T. Genty (✉) · B. Bussière
Department of Applied Sciences, UQAT,
Rouyn-Noranda, QC J9X 5E4, Canada
e-mail: thomas.genty@uqat.ca

T. Genty · B. Bussière · M. Benzaazoua · G. J. Zagury
Industrial NSERC-Polytechnique-UQAT Chair,
Environment and Mine Waste Mgmt, Rouyn-Noranda,
QC J9X 5E4, Canada

M. Benzaazoua
Laboratoire de Génie Civil et d'Ingénierie Environnementale,
INSA de Lyon, 69621 Villeurbanne Cedex, France

G. J. Zagury
Department of Civil, Geological, and Mining Engineering,
École Polytechnique de Montréal, Montreal,
QC H3C 3A7, Canada

$[SO_4^{2-}]$ = 9,000 mg L^{-1} and [Fe] = 4,000 mg L^{-1}). The neutralization was effective for all columns and metal removal efficiencies were, on average, over 90 % for Al, Cd, Cr, Ni, and Zn. Nevertheless, iron removal in the tested AMD did not exceed approximately 20 %. The high iron concentration in the columns' effluents resulted in a high acidity (Kirby and Cravotta 2005), which decreased the pH from 6 to below 4.5 after 8 h of contact with air. Single-step SRPBs can significantly improve water quality but cannot totally remove the contaminants from a high-iron AMD. Therefore, it may be necessary to combine them with other treatment methods to reach environmental targets for highly concentrated AMD (Champagne et al. 2005). Iron removal was studied by Champagne et al. (2005) using a sorption step in a peat filter. Then, a SRPB, ALD, and a settling pond allowed them to adequately treat the AMD (pH of 3.2; iron concentration of 189 mg L^{-1}).

Although not often used in conventional AMD passive treatment systems, adsorbent materials can remove metals from AMD (e.g. Champagne et al. 2005; Polat et al. 2002; Vadapalli et al. 2008). In the present study, wastes from wood combustion (a by-product of a co-generation energy power plant), hereafter called wood ash filters, were tested for their ability to remove iron from highly concentrated AMD because of their local availability and their high carbon content. The wood ash (both bottom and fly ash) is considered to be a waste but has a good valorization potential. The sorption properties mainly come from amorphous iron and aluminium hydroxides, carbon, oxi-hydroxides, carbonated material, and silicate materials (Gonzalez et al. 2009). Biomass ash and particularly wood ash, such as was used in the present study, contain a lot of unburned material, but are not as well characterized in the literature as coal and petroleum coke fly ash (Ahmaruzzaman 2010).

The main objective of the present study was to evaluate the capacity of wood ash filters for use in a polishing step after SRPB treatment of high-iron (approximately 4,000 mg L^{-1}) AMD. Materials were characterized and sorption properties toward iron were determined; iron was selected because it was the most problematic element (see Genty 2012). Then, column tests were carried out to identify retention mechanisms in more realistic conditions and a saturated hydraulic conductivity investigation was performed to evaluate the risk of clogging.

Materials and Methods

Water Quality of the Influent Columns

The wood ash filters influent was the effluent of a laboratory-scale SRPB; it had low metal concentrations except for Mn and Fe (Table 1), which were not efficiently removed by the tested SRPBs (Genty 2012; Neculita et al. 2008a, b), and had a relatively acidic pH (approximately 4) due to the precipitation of iron hydroxides following exposure to atmospheric oxygen (Genty 2012).

Materials

The wood ash used to treat the contaminated drainage from the SRPB is a by-product from a co-generation plant (located at Kirkland Lake, Canada) that uses wood waste to produce energy; it is readily available in our region. The ash, which is a mixture of bottom and fly ash, contains a significant portion of carbon and gravel. Two other materials were obtained from wood ash to evaluate their capacity to treat AMD. The first material, named carbon wood ash, was obtained by processing wood ash in water and by collecting floating particles by flotation. The second material (wood ash less than 1.18 mm in diameter) was obtained by screening dry wood ash in a 1.18 mm sieve. These two materials allowed us to evaluate the role of carbon and fine particles in the neutralization and metal removal processes.

The wood ash, carbon wood ash, and fine wood ash (below 1.18 mm diameter) were characterized to determine their physical and chemical properties.

Specific gravity (G_s) was measured with a helium Micromeritics Accupyc 1330 pycnometer and the specific surface area (S_s) by a Micromeritics Gimini III 2375 surface analyser on dry samples (nitrogen adsorption with BET method). Particle size analysis was carried out using sieves having different openings (Aitcin et al. 1983). The pH was determined in deionized water using a solid to liquid ratio of 1:10 (ASTM 1995a). Total carbon (TC) was measured under oxygen atmosphere with an ELTRA PC-controlled CS2000 carbon sulphur determinator. Total organic carbon (TOC) was measured by adding potassium bichromate and sulphuric acid and measuring excess potassium bichromate; total inorganic carbon (TIC) was calculated as the difference between TC and TOC. Solids were digested in HNO_3, Br_2, HCl, and HF and the liquid resulting from this treatment was analysed for elemental composition by inductively coupled plasma-atomic emission spectrometry (ICP-AES) (Perkin Elmer OPTIMA 3100 RL; relative precision of 5 %).

An X-ray diffractometer (XRD) Bruker axs D8 ADVANCE was used to identify the mineralogy of the crystalline fraction of the tested materials. Samples for XRD were crushed by micronization; the diameter of the powder obtained was approximately 10 μm. The XRD instrument is equipped with a Cu anticathode and scintillation counter. Data treatment was done using a Bruker A.X.S. EVA software package. A thermogravimetric analysis (TGA) coupled with a differential scanning calorimetric analysis (DSC) was performed on each material to complement the

Table 1 Average concentrations (in mg L^{-1} except pH) and standard deviations of the main metals in the polishing column influent (SPRB effluent)

Elements	Average	Standard deviation
Fe	2,972.1	707.9
Mg	30.9	14.6
Mn	33.4	5.0
Ni	0.1	0.1
Pb	0.3	0.1
SO_4^{2-}	8,640	1,025.2
Zn	1.1	0.5
pH	4.0	0.6

mineralogical information. Samples were heated from ambient temperature to 1,000 °C at 20 °C per minute under a nitrogen atmosphere. The main advantage of this technique is that crystalline and amorphous phases can be studied simultaneously. Finally, cationic exchange capacity (CEC) evaluation consisted of saturating all exchange sites with sodium ions (with a 1 N sodium acetate solution) and then desorbing it with a 1 N ammonium acetate solution (adapted from Zagury et al. 2004). Sodium concentration was analysed using a Metrohm 881 compact IC pro ions chromatograph (column Metrosep C415/40, elluent: 1.7 mmol HNO_3 and 0.7 mmol dipicolinic acid, flow rate: 0.9 mL min^{-1}).

Sorption Experiments

Sorption Isotherm and Sorption Kinetic Models

The two most common isotherm models, the Langmuir and Freundlich equilibrium isotherms (Al-Degs et al. 2006; García-Mendieta et al. 2009; Jha et al. 2008), were evaluated in this work. The linear form of the Langmuir equation can be represented by the following equation:

$$\frac{C_e}{q_e} = \frac{1}{b.q_{\max}} + \frac{C_e}{q_{\max}} \quad (1)$$

where C_e is the equilibrium concentration of remaining metal in the solution (mg L^{-1}), q_e is the amount of a metal adsorbed per unit mass of sorbent at equilibrium (mg g^{-1}), q_{max} is the amount of adsorbate at complete monolayer coverage (mg g^{-1}), and b (L mg^{-1}) is a constant related to the heat of adsorption. Freundlich linear isotherm can be expressed by the following expression:

$$\log q_e = \log k_f + n.\log C_e \quad (2)$$

k_f is the equilibrium constant (mg g^{-1}) indicative of adsorption capacity, and n represents the sorption equilibrium constant.

Sorption kinetic models can be divided into two main types: reaction-based models and diffusion-based models (Al-Degs et al. 2006; García-Mendieta et al. 2009; Ho et al. 2000; Jha et al. 2008). Equations 3, 4, and 5 represent three different sorption variations for the reaction-based model:

$$\text{Pseudo first order: } \log(q_e - q_t) = \log\ q_e - k_1.\frac{t}{2.303} \quad (3)$$

$$\text{Pseudo second order: } \frac{1}{q_e - q_t} = \frac{1}{q_e} + k_2.t \quad (4)$$

$$\text{Pseudo second order for chemisoprtion: } \frac{t}{q_t} = \frac{1}{k_3.q_e^2} + \frac{t}{q_e} \quad (5)$$

where q_t is the amount of a metal adsorbed per mass unit of sorbent (mg g^{-1}) at time t (s), k_1 is the pseudo first order rate constant (s^{-1}), k_2, and k_3 the pseudo second order rate constant (g/mg/s^{-1}).

Diffusion-based models can be divided into those controlled by external or internal diffusion. If the external or internal diffusion of metal cations is the rate-limiting step in metal sorption, the kinetic reactions can be represented respectively by:

$$\text{External diffusion: } \ln\frac{C_t}{C_i} = -k_f.\frac{A}{V}.t \quad (6)$$

$$\text{Internal diffusion: } q_t = k_d.t^{1/2} \quad (7)$$

with C_i representing the initial concentration of metal in the solution (mg L^{-1}), C_t the concentration at the time t, k_f and k_d being the external and internal diffusion coefficient (respectively in cm s^{-1} and mg/g^{-1}/$s^{-1/2}$), A representing the external surface of absorbent (cm^2), and V the volume of adsorbant (cm^3).

Sorption Isotherm and Kinetics Experiments

Two g of adsorbent (wood ash, carbon wood ash, or wood ash below 1.18 mm diameter) were weighed and placed into 125 mL Erlenmeyers flasks. For the isotherm experiments, 100 mL AMD solutions of different concentrations (from AMD to AMD diluted fifty times) were prepared and then transferred into the sample bottles. Diluted AMD solution with numerous metal salts (Limousin et al. 2007) was used in the batch tests rather than deionised water with a known iron concentration, even though just iron concentration was measured, since ionic competition can occur on sorption sites. The selected quantity of solid material and solution insured that an equilibrium condition was reached and that the entire metal ion was not adsorbed, so that the equilibrium point could be determined (Gupta et al. 2009).

For the kinetics experiments, 100 mL aqueous solutions of AMD were transferred into the sample bottles. The sample Erlenmeyer flasks were placed on a rotating table (200 rpm) at 21 °C. Experiments were conducted at pH 3 and 6; pH adjustment was performed by adding NaOH 1 N or HCl 1 N solutions. Samples for isotherms experiments were filtered (0.45 μm) after reaching equilibrium for 24 h and analyzed for metals by ICP-AES. Sorption capacity q_e (mg g^{-1}) of the sorbent was calculated by the mass balance Eq. (8) (Al-Degs et al. 2006):

$$q_e = [C_i - C_e].\frac{V}{m} \quad (8)$$

where C_i, C_e, V, and m respectively represent initial metal concentration (mg L^{-1}), metal concentration at equilibrium (mg L^{-1}), total volume (L), and weight (g) of sorbent. Water samples for the kinetics experiments were taken and filtered (0.45 μm) for metal concentration determination at 0, 0.5, 3, 7 and 28 h. Additional data on FTIR characterization of material after sorption tests are given in Online Resource 1, which is available in the electronically published version of this paper, and can be downloaded for free by all journal subscribers.

Column Experiments

Five 1.6 L columns (20 cm in height and 10.5 cm in diameter; see Fig. 1 for a schematic representation) were made to determine the capacity of wood ash to improve water quality (particularly to remove iron) after a sulphate reducing passive biofilter. Polishing columns filled with five different mixtures were investigated (Table 2). These mixtures were chosen to determine the influence of the type of fly ash (carbon and fraction below 1.18 mm diameter) and sand proportion on iron removal and column clogging. The sand used in some of the mixtures was 97 % silica and had the following particle size characteristics: D_{10} (D_x is the effective diameter, corresponding to x% passing on the cumulative grain-size distribution curve) of 0.22 mm, a D_{50} of 0.32 mm, and a uniformity coefficient ($C_U = D_{60}/D_{10}$) of 1.7.

Polishing columns were fed with the SRPB effluent by a peristaltic pump (from bottom to top at a constant flow rate of 0.1 mL min^{-1}). SRPB column tests are presented in Genty (2012). The base of the columns was made of a perforated plastic plate covered by geotextile. The porosity was estimated with the water volume needed to fill up the column totally; porosity values varied from 0.68 to 0.44, as shown in Table 2. Considering a flow rate of 0.1 mL min^{-1}, the hydraulic retention time (HRT) were 5.0 days for column #4, 5.1 days for column #5, 5.3 days for column #1, 6.6 days for column #3, and 7.8 days for column #2.

Analytical Method for Water Quality Evaluation

The pH, Eh, sulphate, acidity, alkalinity, and metal concentrations of influents and effluents were determined during the experiment. The pH was determined with an Orion Triode sensor coupled with a Benchtop pH/ISE Meter Orion model 920 (relative precision ± 0.01 pH) and Eh (redox potential, values were corrected relative to the standard hydrogen electrode) was measured by a Pt/Ag/AgCl sensor linked to a Benchtop pH/ISE Meter Orion 920. The alkalinity concentration was obtained by titration on non-filtered sample with sulphuric acid 0.02 N (precision of 1 mg $CaCO_3$ L^{-1}) until the end-pH of 4.5 and the acidity concentration by titration on non-filtered sample with sodium hydroxide 0.1 N (precision of 1 mg $CaCO_3$ L^{-1}) until the end-pH of 8.3. Filtered samples (0.45 μm filter) used to quantify metal content were acidified with 2 % (by volume) of 70 % nitric acid before analysis by ICP-AES. Sulphate determination assumed that all sulphur was present as sulphate (sulphate concentrations was obtained by multiplying sulphur concentration by the ratio of sulphate molar mass to sulphur molar mass, Potvin 2009). Thermodynamic modeling confirmed this hypothesis since no sulphur species was suggested with the observed experimental conditions.

Saturated Hydraulic Conductivity Evaluation

To quantify possible clogging of the tested systems, saturated hydraulic conductivity k_{sat} was evaluated monthly on the columns during the operation using the falling head method (adapted from ASTM 1995b). Values of k_{sat}

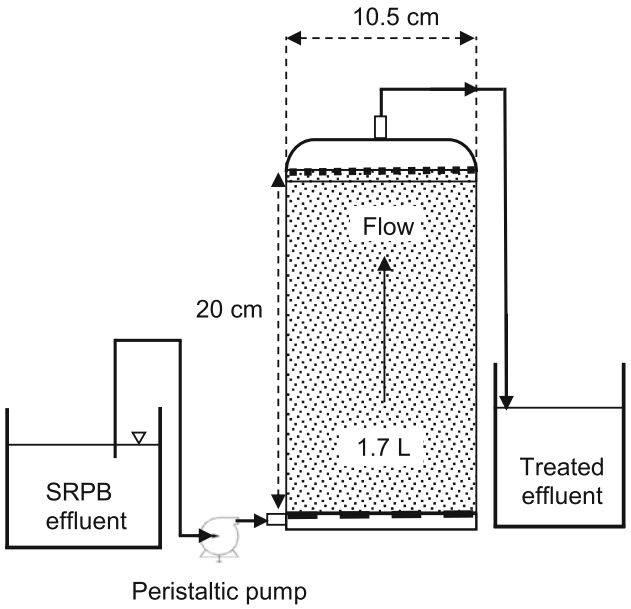

Fig. 1 Polishing column test configuration (fig. not to scale)

Table 2 Polishing column mixture composition (% w/w dry) and characteristics

Mixture	#1	#2	#3	#4	#5
Mixture composition					
Wood ashes	100 %			40 %	70 %
Carbon wood ashes		100 %			
Wood ashes (below 1.18 mm diameter)			100 %		
Sand				60 %	30 %
Column characteristics					
Column number	#1	#2	#3	#4	#5
Mixture mass (dry g)	1,089	471	1,027	1,537	1,408
Height (cm)	20	20	20	20	20
Estimated porosity	0.47	0.68	0.57	0.44	0.44
Estimated HRT (days)	5.3	7.8	6.6	5.0	5.1

(cm s^{-1}) were calculated with the following equation (e.g. McCarthy 1977):

$$k_{sat} = \frac{aL}{At}\ln\left(\frac{h_1}{h_2}\right) \quad (9)$$

where a (cm^2) is the area of the water head column, L (cm) the length of the sample, A (cm^2) the area of the sample, and t (s) the time necessary for the water head column to drop from head h_1 (cm) to h_2 (cm).

Columns Post-testing Characterisation

At the end of the experiment, samples were collected at 10 cm (from the top) for each reactor. Samples were quickly frozen to prevent metal speciation changes. Metal fractionation in the five tested mixtures was estimated with a semi-quantitative sequential extraction procedure (SEP, Neculita and Zagury 2008; Zagury et al. 1997), as described in Online Resource 2.

To evaluate the mineralogy of solid crystalline phases produced in the columns, XRD analyses were carried out on samples from each column. Material was also quickly sampled and then frozen to prevent changes of metal speciation at the end of the experiment. These samples were thawed under nitrogen flow to prevent mineralogical changes. A Hitachi 3,500-N scanning electron microscope (SEM) with the secondary electron mode coupled with an energy dispersive spectrometry (EDS) of an X-ray probe (voltage of 20 keV, amperage of 140 A, pressure around 25 kPa, and a work distance of 15 mm) was used to characterize the microstructure, texture, and chemistry of samples. The samples were then chemically analysed, as discussed above.

Finally, chemical speciation at equilibrium was estimated using the composition of column effluents. Saturation index of the main minerals susceptible to precipitate were calculated using a thermodynamic chemical equilibrium model (Vminteq v 2.53) with the activity correction proposed in the SIT model and the MINTEQA2 data base (KTH 2010). Redox potential versus pH diagram was also determined using JCHESS version 2.0 (Van Der Lee 1993) to better visualize the iron and sulphate behaviour in the columns. The temperature selected to construct the graph was 21 °C (laboratory temperature), and average iron and sulphate concentrations of each columns were used.

Characterization Results

Materials Characterisation

Physical and chemical characteristics of the reactive materials are showed in Table 3. As expected, the fine fraction wood ash (below 1.18 mm diameter) had the smallest particle size distribution (D_{10} of 0.09 mm and D_{50} of 0.45 mm) and the highest specific gravity ($G_s = 2.70$). Carbon wood ash had a G_s of 2.55 and had the coarsest particle size distribution (D_{10} of 0.66 mm and D_{50} of 1.15 mm). Woods ash specific gravity was 1.74. Each material contained non-negligible TOC (between 12 % for wood ash below 1.18 mm diameter and 32 % for carbon wood ash), since all three contained a significant proportion of unburned wood (as seen visually in the material). Unburned wood was directly linked to the TOC content since unburned wood has a TOC content close to 50 % (Genty 2012) and carbon wood ash had the highest TOC (64 %) because of the preparation method (wood ash concentration by collectorless flotation). S_s values were approximately 46 $m^2\ g^{-1}$ for wood ash, 159 $m^2\ g^{-1}$ for the carbon wood ash, and 52 $m^2\ g^{-1}$ for the wood ash below 1.18 mm diameter. These relatively high specific surface areas should provide good sorption ability.

Wood ash had a higher pH than the other wood ash materials studied: 12.2 compared to 9.9 for carbon wood ash and 10.3 for wood ash below 1.18 mm diameter. Digestion of materials and analysis of metal content showed that calcium was an important element (12.3 % for wood ash, 14.0 % for carbon wood ash, and 7.2 % for wood ash below 1.18 mm diameter). However, digestion was not complete because some particles were not totally dissolved at the end of the preparation. Mineralogical quantification by XRD could not be done on the initial material because it was largely amorphous. Nevertheless, XRD showed that quartz and calcite were significantly present in the crystalline fraction of the three materials; the presence of calcite was in accordance with the relatively high calcium concentration (between 7.23 and 14 %) determined by ICP-AES on the solid samples. Other minerals identified by XRD in the materials included: silicates (muscovite, albite, anorthite, actinolite, chlorite, microcline), sulphate (gypsum), oxides (rutile), carbonates (siderite), and sulphur. Silicates, oxides, sulphate, silica, and carbonates have been identified in fly ash from different sources (Gonzalez et al. 2009). The TGA-DSC thermal analysis performed on the three initial wood ash materials allowed us to determine which material had the highest calcite content. The differential weight loss curve and the DSC signal showed two main endothermic weight losses, at 82–88 °C and 753–767 °C. The loss at 82–88 °C was probably due to water release because samples were dried at only 40 °C before analysis. Between this temperature and 700 °C, a regular loss of weight appeared for each material, corresponding to the decomposition of organic unburnt materials present initially. The last reaction, at 753–767 °C, is due to calcite decarbonatation (CO_2 release, Ouellet et al. 2006). Results showed a weight loss of 6.9 % for wood ash, 6.8 % for carbon wood ash, and 10.1 % for wood ash below 1.18 mm diameter. These last results showed that wood ash below 1.18 mm diameter probably have the highest carbonate content, contradicting the ICP results, probably because of the partial chemical digestion mentioned earlier (the hypothesis here is that calcium is present only as a carbonate mineral).

Sorption Batch Test Results and Iron Retention

Table 4 presents the fitting of Langmuir and Freundlich models with experimental isotherm data. The Freundlich model more appropriately represented the obtained isotherms for both tested pHs, 3 and 6, and for the three wood ash materials tested. This indicates that the sorption occurs on a heterogeneous surface (Jha et al. 2008). Furthermore, the isotherm results showed that iron removal was more important at pH 3 than at pH 6, with higher k_f values (k_f represents the adsorbed quantity of iron in mg g^{-1} of material, for an iron equilibrium concentration of 1 mg L^{-1}), and that wood ash below 1.18 mm diameter had the highest iron retention capacity.

Sorption phenomena can also be described by kinetic sorption tests. The equilibrium capacity (q_e) has been determined in order to use kinetic models presented in Eqs. (3), (4). The values of q_e were calculated from the Freundlich equation. The equilibrium concentration C_e can

Table 3 Reactive material characteristics

	Wood ashes	Carbon wood ashes	Wood ashes below 1.18 mm diameter
Physical characteristics			
D_{50} (mm)	0.60	1.15	0.45
D_{10} (mm)	0.11	0.66	0.09
Specific gravity	1.74	2.55	2.70
Specific surface area (m^2 g^{-1})	46.03	158.77	51.60
Chemical characteristics			
Total carbon (% dry)	36	64	31
Total organic carbon (% dry)	19	32	12
Total inorganic carbon (% dry)	17	32	19
pH	12.2	9.9	10.3
Element abundance by ICP-AES			
Al (wt%)	2.3	2.1	0.5
Ca (wt%)	12.3	14.0	7.2
Fe (wt%)	1.5	1.4	0.4
Mg (wt%)	1.4	1.3	0.6
Mn (wt%)	0.2	0.3	0.1
S (wt%)	0.2	0.2	0.1

be represented by the following equation (Al-Degs et al. 2006):

$$C_e = C_0 - C_{surface} \quad (10)$$

where C_0 and $C_{surface}$ are, respectively, the initial concentration of iron (mg L^{-1}) and the surface concentration at equilibrium (mg L^{-1}). The ratio of the sorbent mass (g) to the volume of the solution (L) can be presented as the parameter m:

$$m = \frac{mass}{volume} \quad (11)$$

The surface concentration ($C_{surface}$) is equal to $m.q_e$. By combining Eqs. (2), (10), and (11), q_e (mg g^{-1}) values were calculated using the following equation:

$$\log(q_e) - \log(k_f) - n.\log(C_0 - m.q_e) = 0 \quad (12)$$

Values of q_e that solved Eq. (12) are called $q_{e,Freundlich}$ and are presented in Table 4. These values were then used to model experimental kinetic data according to Eqs. (3) to (5).

Table 5 shows that several kinetic models can fit the experimental data with a high correlation coefficient for most materials at the two tested pHs. The selection of the most appropriated kinetic model was made by calculating the sum of square of the errors (SSE), according to Al-Degs et al. (2006) and Cheung et al. (2000).

$$SSE = \sum (q_{t,\exp} - q_{t,theo})^2 \quad (13)$$

where $q_{t,\exp}$ and $q_{t,theo}$ are the experimental sorption capacity of iron (mg g^{-1}) at time t and the corresponding value obtained with the kinetic models, $q_{t,theo}$, was determined using kinetic models according to the parameters of Table 5 and Eqs. (3)–(7). The model with the lower SSE value can give an indication of the sorption limiting step (Al-Degs et al. 2006; Cheung et al. 2000). According to the SSE values, the model that best represents the sorption kinetic for wood ash and carbon wood ash at pH 3 and wood ash below 1.18 cm at pH 6 was a pseudo second order reaction (Eq. (5). This reaction is typical of a chemisorption reaction (Ho et al. 2000). For wood ash and carbon wood ash at pH 6 and fine wood ash (below 1.18 mm) at pH 3, the kinetic limiting step seemed to be the diffusion of iron to the sorption site. This diffusion could be external (Eq. (6), wood ash, pH 6), i.e. the surface process occurred on the exterior of the sorbent particle, (Eq. (7), carbon wood ash, pH 6 and wood ash below 1.18 mm, pH 3) or internal, i.e. the process of sorption is controlled by a migration of iron ions inside the sorbent particle (Al-Degs et al. 2006).

Sorption of metal onto a material surface is complex and numerous mechanisms can occur, such as adsorption (physisorption or chemisorption), cationic exchange, and surface precipitation. Isotherms and kinetic tests characterization, respectively, allow one to describe the sorption mode (sorption onto a homogeneous or heterogeneous surface) and to determine if the diffusion of metal or the reaction at the surface is the limiting step during the sorption mechanism. However, the type of interaction between the metal and the sorption site cannot be specifically identified with these two common approaches.

A positive CEC shows that the interaction between metal and the sorption site is an ionic link. The measured CEC values for the reactive materials showed that ion exchange is one of the main sorption phenomena that explain iron retention in the three tested wood ash materials. CEC values were 24.9 meq/100 g (dry) for wood ash, 49.8 meq/100 g (dry) for carbon wood ash, and 12.8 meq/100 g (dry) for wood ash below 1.18 mm diameter. These values are in the same range as those observed for organic material like compost (53.2 meq/100 g, Karathanasis et al. 2010), but significantly lower than those of peat (119.5 meq/100 g, Twardowska and Kyziol 2008), which is recognized as having a significant CEC (Twardowska and Kyziol 2008). Indeed, activated carbons, which are close to the tested material of this study, are usually considered to not have a high exchange capacity (Johnson et al. 1986).

Table 4 Iron sorption isotherm models for pH 3 and 6 on the three wood ash materials studied

Isotherm models	pH 3					pH 6				
	Best fit model	R^2	k_f (mg g^{-1})	n	$q_{e,Freundlich}$ (mg g^{-1})	Best fit model	R^2	k_f (mg g^{-1})	n	$q_{e,Freundlich}$ (mg g^{-1})
Wood ashes	Freundlich	0.81	16.62	0.14	49.37	Freundlich	0.97	8.41	0.21	38.96
Carbon wood ashes	Freundlich	0.78	14.87	0.28	108.23	Freundlich	0.99	4.36	0.43	75.30
Wood ashes below 1.18 mm diameter	Freundlich	0.68	81.65	0.64	168.30	Freundlich	0.99	23.68	0.60	112.35

Calculated q_e (mg g^{-1}) values calculated with Eq. (12) are noted in the paper as $q_{e,Freundlich}$. At pH 3, C_0 was 3370 mg L^{-1} and at pH 7 2260 mg L^{-1}. m value was 20

Table 5 Iron sorption kinetic models for pH 3 and 6 on the three wood ash materials studied

Material	pH 3		Kinetic reaction models				Diffusion reaction models	
	Kinetic model	R^2	k_1 (h^{-1})	k_2 (g mg h^{-1})	k_3 (g mg h^{-1})	q_e (mg g^{-1})	k_f.A/V (cm h^{-1} cm^2 cm^{-3})	k_d (mg g^{-1} $h^{-1/2}$)
Wood ashes	Pseudo second order Eq. (5)	0.99	–	–	0.0032	126.58	–	–
Carbon wood ashes	Pseudo second order Eq. (5)	0.99	–	–	0.0029	133.33	–	–
Wood ashes < 1.18 mm diameter	Pseudo first order Eq. (3)	0.99	0.093	–	–	8.60	–	–
	Pseudo second order Eq. (5)	0.97	–	–	0.012	181.82	–	–
	External diffusion Eq. (6)	0.98	–	–	–	–	0.10	–
	Internal diffusion Eq. (7)	0.98	–	–	–	–	–	30.18
Material	pH 6		Kinetic reaction models				Diffusion reaction models	
	Kinetic model	R^2	k_1 (h^{-1})	k_2 (g mg h^{-1})	k_3 (g mg h^{-1})	q_e (mg g^{-1})	k_f.A/V (cm h^{-1} cm^2 cm^{-3})	k_d (mg g^{-1} $h^{-1/2}$)
Wood ashes	Pseudo second order Eq. (5)	0.99	–	–	0.023	123.46	–	–
	External diffusion Eq. (6)	0.99	–	–	–	–	0.148	–
	Internal diffusion Eq. (7)	0.91	–	–	–	–	–	21.66
Carbon wood	Pseudo first order Eq. (3)	0.99	0.092	–	–	6.39	–	–
ashes	Pseudo second order Eq. (4)	0.97	–	0.0062	–	294.12	–	–
	External diffusion Eq. (6)	0.91	–	–	–	–	0.036	–
	Internal diffusion Eq. (7)	0.99	–	–	–	–	–	13.29
Wood ashes < 1.18 mm diameter	Pseudo second order Eq. (5)	0.99	–	–	0.0035	123.46	–	–
	External diffusion Eq. (6)	0.93	–	–	–	–	0.360	–

Only best fit model (with $R^2 > 0.90$), are presented

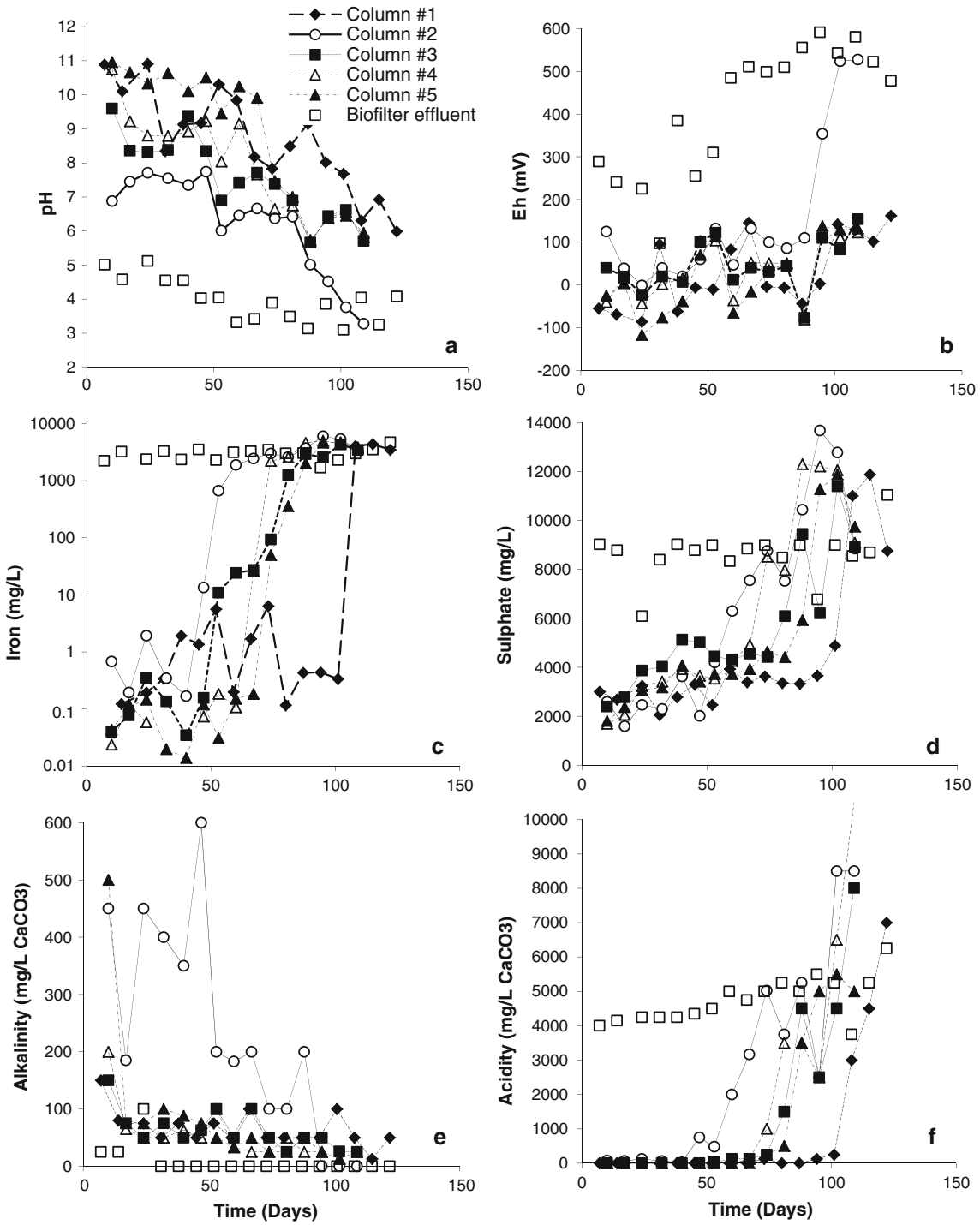

Fig. 2 Polishing column chemical parameters: **a** pH, **b** Eh (mV), **c** iron concentration (mg L^{-1}), **d** sulphate concentration (mg L^{-1}), **e** alkalinity (mg L^{-1} eq. $CaCO_3$) and **f** acidity (mg L^{-1} eq. $CaCO_3$)) for all column tests studied

Column Treatment Performance

Treatment with Wood Ash After a Sulphate-reducing Biofilter

The pH in the polishing column effluents rose initially to approximately 11 for columns containing 100 % (column #1), 70 % (column #5), and 40 % (column #4) wood ash. For wood ash below 1.18 mm diameter (column #3) and carbon wood ash (column #2), pH increased initially up to 8–10 and 7–8, respectively (Fig. 2a). Then, pH decreased progressively with time to a value of approximately 6 for all columns except for column #2, which maintained a pH close to that of the SRPB effluent (average pH = 3.5) at

the end of the experimental period. Decreased pH is probably due to the disappearance of alkaline minerals like calcite during the first step of the experiment. The redox potential (Eh) value decreased between −100 and 100 mV for each column (Fig. 2b). The ashes helped to maintain a redox potential between −100 and 100 mV due to their neutralization capacity; a similar behaviour is observed with neutralization by carbonate minerals (see Potvin 2009). However, the values tended to increase with time; for column #2, Eh increased rapidly after 80 days to reach the value observed at the SRPB effluent column. This increase of Eh is linked to the drop in pH (below 5 after 80 days) due to the lack of neutralization capacity. Biofilter effluent pH and Eh evolved with time due to the acidification that occurred in the feed tank (value stabilized after approximately 40 days). This acidification is due to the hydrolysis and precipitation of iron (Genty et al. 2012).

Iron concentrations decreased from approximately 2,972 mg L^{-1} for the SRPB effluent to below 7 mg L^{-1} during the first 108 days for column #1 (see Fig. 2c). Then, iron concentration increased rapidly to reach the initial SRPB effluent iron concentration. A similar trend was observed for the other columns but the breakthrough time to reach the SRPB effluent values was different: 20, 53, 60, and 67 days, respectively (before this date, iron concentration was below 1 mg L^{-1}) for columns #2, 3, 4, and 5. The number of pore volumes (see Online Resource 3) necessary to saturate sorption sites with iron was estimated at 20, 14, 13, 9, and 6 days, respectively, for columns #1, 5, 4, 3, and 2. This means that the treatment life of a polishing treatment step was significantly affected by the type of wood ash material used.

Sulphate retention was effective before the breakthrough time with a decrease from average values higher than 8,640 mg L^{-1} for the SRPB effluent to below 4,869, 4,200, 4,422, 4,920, and 4,416 mg L^{-1}, respectively, in columns #1, 2, 3, 4, and 5 (see Fig. 2d). The breakthrough time was approximately 108, 81, 74, 60, and 53 days for columns #1, 5, 3, 4, and 2, respectively. After this period, sulphate concentrations increased to values similar to those observed in the SRPB effluent. A release of sulphate was also observed at the end of the experimental period since concentrations at the effluent of all polishing columns exceeded the influent concentration. More details on iron and sulphate stability phases are presented in Online Resource 4 using an Eh–pH stability diagram.

Alkalinity (Fig. 2e) was generated in each column, with higher values for columns containing carbon wood ash (average value of 227 mg L^{-1} $CaCO_3$ for column #2, and between 53 and 80 for the other four columns). Acidity evolution (see Fig. 2f) was related to iron concentration at the exit of the polishing columns. Indeed, acidity increased from low values before the breakthrough time for iron to values similar to the SRPB effluent, and even higher, at the end of experiment.

A breakthrough can also be observed for the other metals present in the SRPB effluent (Mn, Ni, Pb, and Zn). Metal retention was relatively effective before this breakthrough time in each column, with concentrations below 10 mg L^{-1} for Mn, 0.1 mg L^{-1} for Ni, 0.3 mg L^{-1} for Pb, and 1 mg L^{-1} for Zn. The breakthrough was observed for Ni, Pb, and Zn at 108 days, 47 days, 74 days, between 67 and 74 days, and between 74 and 81 days for columns #1, 2, 3, 4, 5, respectively. The breakthrough happened for Mn at the same time as for the previous metals for columns #1, 2, and 5 (respectively 108, 47, and between 67 and 74 days). The breakthroughs for columns #3 and 4 occurred after 40 and 47 days, respectively. After the breakthrough, effluent metal concentrations of polishing columns reached the concentrations of the initial SRPB effluent.

Saturated hydraulic conductivity (k_{sat}) is useful in evaluating the long term performance of filters and particularly to quantify the clogging phenomena (Seki et al. 2006; Soleimani et al. 2009). Saturated hydraulic conductivity k_{sat} stayed relatively stable for each column, between 5.0×10^{-3} and 3.1×10^{-2} cm s^{-1}. These values seemed to indicate that the columns did not clog during treatment. Moreover, high values of k_{sat} measured during the test showed that the materials were relatively permeable (values similar to sandy materials, Chapuis 2004).

The polishing column containing only wood ash had the best treatment performance: metal retention was effective for the longest period (compared to the other materials) while a saturated hydraulic conductivity similar to those of wood ash containing sand was maintained (said differently, adding sand to the studied wood ash was not necessary to avoid clogging of the system). Moreover, adding sand did not significantly affect the HRT (columns #1, 4, and 5 had similar HRTs), but affected the treatment performance; column #1 was more efficient in removing iron than columns #4 and 5.

Performance was related to the material used. Indeed, the least effective column was the one containing carbon wood ash. This material was mainly composed of coarse carbon particles and had a paste pH close to 9. Initial wood ash material had the highest paste pH (near 12). This high alkaline potential could come from amorphous minerals (not identified by the techniques used). Precipitation can be an important iron retention mechanism when a material has a high paste pH. Wood ash below 1.18 mm diameter had an intermediate paste pH and consequently, an intermediate performance. Moreover, adding sand to two columns did not improve their retention performance since sand can be considered inert towards metal retention; the higher the sand percentage in the column, the lower the efficiency.

Metal Retention Mechanisms

According to the literature, metal retention in wood ash materials occurs in different ways. Aluminium removal mainly comes from the precipitation of amorphous hydroxides at a pH above 5 (Vadapalli et al. 2008). Other metals, like Ni, Zn, Pb, Cr, and Cd, can be removed by precipitation, co-precipitation, sorption onto the surface of fly ash, and sorption onto amorphous Fe, Al hydroxides and oxohydroxide (Ahmaruzzaman 2010; Gitari et al. 2006, 2008; Gonzalez et al. 2009; Polat et al. 2002; Vadapalli et al. 2008). XRD analysis of samples taken from the five columns post-testing confirmed the precipitation of magnesite (magnesium carbonate) for column #3, goethite (iron oxyhydroxide), and diaspore (aluminum oxyhydroxide) for column #1.

In all columns, precipitation of a calcium sulphate occurred as anhydrite. Indeed, the literature shows that sulphate can be removed by formation of calcium sulphate, like gypsum or ettringite in fly ash materials (Madzivire et al. 2010; Reynolds and Petrik Reynolds Petrik 2005; Vadapalli et al. 2008), but also by sorption onto iron hydroxide and oxi-hydroxi-sulphate (Gitari et al. 2006; Vadapalli et al. 2008). Moreover, the XRD calcite line intensity decreased, which is probably due to calcite dissolution during treatment. This observation is confirmed by the total calcium content in the post-testing samples, which decreased between 0.7 and 12.2 %, depending on the column (Table 6). Iron content increased between 0.6 and 6.4 %, and sulphide increased between 0.9 and 2.7 % depending on the column (Table 6). In addition, modelling using Vminteq at 10 days suggested a precipitation of carbonate (calcite, magnesite, dolomite, and rhodochrosite) and hydroxides (geothite, lepidochrocite, and ferrihydrite) in the five polishing columns. However, at the end of the experiment (109 days), only the precipitation of geothite, lepidochrocite, ferrihydrite, and siderite was possible, according to thermodynamic modeling (see Table 6).

Metal fractionation results are summarized in Online Resource 5. The sequential extraction procedure fractionated metals into: soluble or exchangeable (fraction 1), carbonate bound (fraction 2), reducible or bound to Fe–Mn oxides (fraction 3), oxidisable or bound to organic matter (fraction 4), or residual (fraction 5) fractions. Iron, which was the most problematic metal to be treated in the tested AMD, was stabilized mainly in the reducible or bound to Fe–Mn oxides-hydroxides fractions (73.4–51.1 %), confirming the possible precipitation of goethite observed in XRD analysis and predicted by geochemical modelling. The same was true for Mn, Pb, and Zn. Oxides or hydroxides forms represent a relatively stable phase for these metals. The second iron retention mechanism in term of percentage was association with organic matter fraction (15–28 %).

The second observation pointed out by the sequential extraction procedure was that the soluble or exchangeable fraction (fraction 1) was not negligible for Mn (between 2.9 and 33.3 %) and Ni (8.3 and 71.8 %). Thus, precautions should be taken to prevent remobilization of Ni and Mn. Moreover, the quantity of soluble or exchangeable phase

Table 6 Summary of the metal retention mechanisms in the tested columns

Characterization techniques	Observations in all columns	Metal retention and neutralization mechanisms
XRD	Magnesite in column #3	Formation of Mg carbonates; formation of Fe et Al. oxy/hydroxides; formation of calcium sulphate; dissolution of Ca carbonate during column tests
	Geothite, diaspore in column #1	
	Anhydrite in all columns	
	Decrease of calcite ray intensity	
Digestion and metal content analysis by ICP-AES	Decreased Ca content between −0.7 and 12.2 %, increased Fe content between 0.6 and 6.4 %, and increased S content between 0.9 and 2.7 %	Dissolution of Ca mineral, retention of Fe, retention of S
Vminteq modeling	At 10 days: precipitation of magnesite, calcite, dolomite, rodochrocite, geothite, lepidochrocite, ferrihydrite	Formation of Fe oxy/hydroxides and carbonates (Mg, Mn, Fe, Ca)
	At 109 days: precipitation of geothite, lepidochrocite, ferrihydrite, siderite	Formation of Fe oxy/hydroxides and Fe carbonates
Metal fractionation	Fraction 3 had for most of the highest metal content	Formation of reducible or bound to Fe–Mn oxides-hydroxides phases
	Non-negligible fraction 1 for Ni and Mn	Ni and Mn was in part soluble or exchangeable
	Non-negligible fraction 1 for carbon wood ashes for every metal	every metal was soluble or exchangeable in a high quantity for carbon wood ashes
SEM–EDS	Fe and O were superimposed	Formation of Fe oxy/hydroxides
	Ca, S and O were superimposed	formation of calcium sulphate (gypsum)

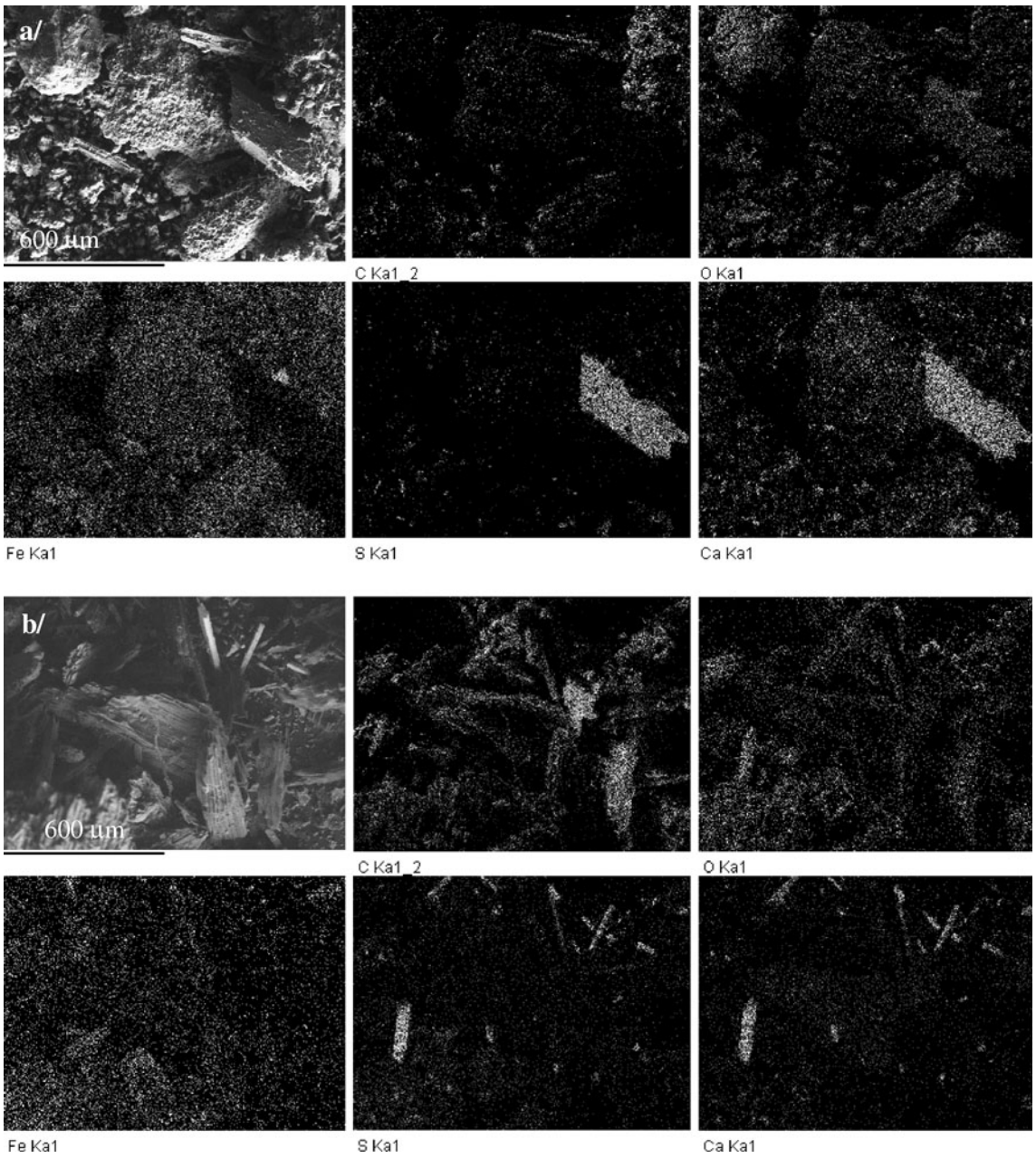

Fig. 3 SEM images and elemental maps: **a** wood ash and **b** carbon wood ash

was always higher for each metal when carbon wood ashes were used as treating material. Thus, use of carbon wood ash filter was not recommended because of the high mobility of most metals retained on this material and because this material had the shortest metal retention efficiency period (see Sect. 4.1).

Finally, SEM observations confirmed the retention of sulphate as gypsum flakes (superposition of Ca, S, and O in Fig. 3b of the carbon wood ash). Iron was probably precipitated as hydroxides or oxyhydroxides since Fe and O was superimposed for wood ash and carbon wood ash (see Fig. 3a, b).

Conclusion

Treatment of high concentrations of iron (e.g. 4,000 mg L^{-1}) in AMD by a sulphate reducing passive biofilter (SRPB) is generally limited. In this study, polishing treatment systems containing different wood ash mixtures (wood ash, 70 % wood ash + 30 % sand, 40 % wood ash + 60 % sand, wood ash below 1.18 mm, and carbon wood ash) were evaluated for a contaminated drainage effluent coming from a SRPB, using five columns. Results showed that acidity can be neutralized and that the column that contained only wood ash had the longest lifetime, over

100 days (corresponding to 20 pore volumes). During this period, iron concentrations decreased from an average of 3,200 mg L^{-1} and did not exceed 10 mg L^{-1}. The iron sorption isotherm correspond to the Freundlich model for wood ash, carbon wood ash, and fine wood ash (below 1.18 mm diameter) at pH 3 and 6. However, the limiting steps of iron sorption depended on material and pH. A pseudo-second order reaction at the surface of material, or internal and external diffusion of iron at the surface of the grain could explain the sorption kinetics. By using the iron retention isotherm for wood ash material, it was possible to estimate the design life of the system at the laboratory scale. Indeed, the design life time for the wood ash column, which performed the best, was estimated at 85 days (considering the mass of wood ash in the columns, the maximum iron retention capacity at 35 mg g^{-1} of wood ash, at pH 6). This value is close to the real value observed in the column, approximately 100 days.

Iron (the most problematic element to be treated in the studied AMD) removal mainly occurred due to hydroxides or oxi-hydroxides precipitation. Indeed, MEB analysis showed a correlation between Fe and O elements on the material surface and XRD analysis of post-testing material, indicating the formation of goethite precipitates. Finally, sequential fractionation indicated that the iron was mainly contained (73.4–51.1 %) in a reducible or bound to Fe–Mn oxides-hydroxides fraction. Sorption could also play an important treatment role, since fraction 4 of sequential fractionation (bound to organic matter phase) was not negligible for each material.

A second important contaminant retained in the columns was sulphate. Indeed, concentrations of sulphate decreased significantly (between 43 and 51 % was removed, depending on the column), mainly by precipitation of calcium sulphate phases (gypsum or anhydrite). Because the wood ash filter system was only efficient for approximately 20 pore volumes to treat an effluent with 3,200 mg L^{-1} of iron on average, the system would have to be changed periodically to maintain an acceptable water quality at the exit of the system. Finally, this study showed that wood ash from a co-generation plant could be a feasible alternative to more traditional materials (e.g. limestone, peat) in passive systems because of its neutralizing potential and metal removal properties.

Acknowledgments This research was supported by the Canada Research Chair on Restoration of Abandoned Mine Sites and the Natural Sciences and Engineering Research Council of Canada (NSERC) through the Industrial NSERC—École Polytechnique—Université du Québec en Abitibi Témiscamingue Chair in Environment and Mine Wastes Management. The authors acknowledge gratefully the industrial and governmental partners of the industrial Chair for the funding of this study and Brian Coghlan from Wood Ash Industries Inc for graciously supplying wood ash.

References

Ahmaruzzaman M (2010) A review on the utilization of fly ash. Prog Eng Combust Sci 36:327–363. doi:10.1016/j.pecs.2009.11.003

Aitcin JC, Jolicoeur G, Mercier M (1983) Technologie des granulats. Les éditions Le Griffon d'Argile, Sainte-Foy

Al-Degs Y, El-Barghouthi M, Issa A, Khraisheh M, Walker G (2006) Sorption of Zn(II), Pb(II), and Co(II) using natural sorbents: equilibrium and kinetic studies. Water Res 40:45–2658. doi:10.1016/j.watres.2006.05.018

ASTM (1995a). Standard test method for pH of soils. In: annual book of ASTM standards, vol 04.08, section D4972-95a, Washington DC, pp 27–28

ASTM (1995b) Standard test method for permeability of granular soils. Annual book of ASTM Standards, vol 04.08, section D, Washington DC, pp 2434–68

Aubertin M, Bussière B, Bernier L (2002) Environnement et gestion des rejets miniers. Edition Presses Internationales Polytechnique, Montréal

Blowes DW, Ptacek CJ (1994) System for treating contaminated groundwater. US Patent 5,362,394, Nov 8, 1994

Champagne P, Van Geel P, Parker W (2005) A bench-scale assessment of a combined passive system to reduce concentrations of metals and sulphate in acid mine drainage. Mine Water Environ 24:124–133. doi:10.1007/s10230-005-0083-1

Chapuis RP (2004) Predicting the saturated hydraulic conductivity of sand and gravel using effective diameter and void ratio. Can Geotech J 41:787–795. doi:10.1139/T04-022

Cheung CW, Porler JF, McKay G (2000) Elovich equation and modified second-order equations for sorption of cadmium ions onto bone char. J Chem Technol Biotechnol 75:963–970. doi:10.1002/1097-4660(200011)75:11<963:AID-JCTB302>3.0.CO;2-Z

Costa MC, Martins M, Jesus C, Duarte JC (2008) Treatment of acid mine drainage by sulphate-reducing bacteria using low cost matrices. Wat Air Soil Pollut 189:149–162. doi:10.1007/s11270-007-9563-1

Cravotta CA, Trahan MK (1999) Limestone drains to increase pH and remove dissolved metals from acidic mine drainage. Ap Geochem 14:581–606. doi:10.1016/S0883-2927(98)00066-3

Deng S, Ting YP (2005) Characterization of PEI-modified biomass and biosorption of Cu(II), Pb(II) and Ni(II). Wat Res 39:2167–2177. doi:10.1016/j.watres.2005.03.033

Evangelou VP, Zhang YL (1995) A review: pyrite oxidation mechanisms and acid mine drainage prevention. Environ Sci Tech 25:141–199. doi:10.1080/10643389509388477

García-Mendieta A, Solache-Ríos M, Olguin M (2009) Evaluation of the sorption properties of a Mexican clinoptilolite-rich tuff for iron, manganese and iron–manganese systems. Micropor Mesopor Mater 118:489–495. doi:10.1016/j.micromeso.2008.09.028

Genty T (2012) Comportement hydrobiogéochimique de systèmes passifs de traitement du drainage minier acide fortement contaminé en fer. PhD Diss, Chaire industrielle CRSNG Polytechnique—UQAT, Rouyn-Noranda, QC, Canada

Genty T, Bussière B, Potvin R, Benzaazoua M, Zagury GJ (2012) Dissolution of different limestone in highly contaminated acid mine drainage: application to anoxic limestone drains. Environ Earth Sci. doi:10.1007/s12665-011-1464-3

Gitari W, Petrik L, Etchebers O, Key D, Iwuoha E, Okujeni C (2006) Treatment of acid mine drainage with fly ash: removal of major contaminants and trace elements. J Environ Sci 41:1729–1747. doi:10.1016/j.fuel.2008.03.018

Gitari W, Petrik L, Etchebers O, Key D, Iwuoha E, Okujeni C (2008) Passive neutralisation of acid mine drainage by fly ash and its derivatives: a column leaching study. Fuel 87:1637–1650. doi:10.1016/j.fuel.2007.08.025

Gonzalez A, Navia R, Moreno N (2009) Fly ash from coal and petroleum coke combustion: current and innovative potential applications. Waste Manag Res 27:976–987. doi:10.1177/0734242×09103190

Gupta B, Curran M, Hasan S, Ghosh TK (2009) Adsorption characteristics of Cu and Ni on Irish peat moss. J Environ Manag 90:954–960. doi:10.1016/j.jenvman.2008.02.012

Hedin RS, Nairn RW, Kleinmann RLP (1994) Passive Treatment of Coal Mine Drainage. US Bureau of Mines, Pittsburgh

Ho YS, Ng JCY, McKay G (2000) Kinetics of pollutant sorption by biosorbent: reviews. Clear Wat Sep Purif Methods 29:189–232. doi:10.1081/SPM-100100009

Jha V, Matsuda M, Miyake M (2008) Sorption properties of the activated carbon-zeolite composite prepared from coal fly ash for Ni^{2+}, Cu^{2+}, Cd^{2+} and Pb^{2+}. J Hazard Mater 160:148–153. doi:10.1016/j.jhazmat.2008.02.107

Johnson DB, Hallberg KB (2005) Acid mine drainage remediation options: a review. Sci Total Environ 338:3–14. doi:10.1016/j.scitotenv.2004.09.002

Johnson JS, Westmoreland CG, Sweeton FH, Kraus KA, Hagaman EW (1986) Modification of cation exchange properties of activated carbon by treatment with nitric acid. J Chromatogr 345:231–248. doi:10.1016/S0021-9673(01)87025-4

Karathanasis AD, Edwards JD, Barton CD (2010) Manganese and sulphate removal from a synthetic mine drainage through pilot scale bioreactor batch experiments. Mine Water Environ 29:144–153. doi:10.1007/s10230-009-0095-3

Kirby CS, Cravotta CA (2005) Net alkalinity and net acidity: theoretical considerations. Appl Geochem 20:1920–1940. doi:10.1016/j.apgeochem.2005.07.002

Kleinmann RLP, Crerar DA, Pacelli RR (1981) Biogeochemistry of acid mine drainage and a method to control acid formation. Mining Eng 300–304

KTH (2010) Visual MINTEQ A free equilibrium speciation model, version 3.0, beta version. http://www.lwr.kth.se/English/OurSoftware/vminteq/index.html, accessed 15 Sept 2010

Limousin G, Gaudet JP, Charlet L, Szenknect S, Barthes V, Krimissa M (2007) Sorption isotherms: a review on physical bases, modeling and measurement. Appl Geochem 22:249–275. doi:10.1016/j.apgeochem.2006.09.010

Madzivire G, Petrik L, Gitari W, Ojumu T, Balfour G (2010) Application of coal fly ash to circum-neutral mine waters for the removal of sulphates as gypsum and ettringite. Miner Eng 23:252–257. doi:10.1016/j.mineng.2009.12.004

McCarthy DF (1977) Essentials of soil mechanics and foundations. Reston Publ, Reston

Neculita CM, Zagury GJ (2008) Biological treatment of highly contaminated acid mine drainage in batch reactors: long-term treatment and reactive mixture characterization. J Hazard Mater 157:358–366. doi:10.1016/j.jhazmat.2008.01.002

Neculita CM, Zagury GJ, Bussiere B (2007) Passive treatment of acid mine drainage in bioreactors using sulphate-reducing bacteria: critical review and research needs. J Environ Qual 36:1–16. doi:10.2134/jeq2006.0066

Neculita CM, Zagury GJ, Bussiere B (2008a) Effectiveness of sulphate-reducing passive bioreactors for treating highly contaminated acid mine drainage: I. Effect of hydraulic retention time. Appl Geochem 23:3442–3451. doi:10.1016/j.apgeochem.2008.08.004

Neculita CM, Zagury GJ, Bussiere B (2008b) Effectiveness of sulphate-reducing passive bioreactors for treating highly contaminated acid mine drainage: II. Metal removal mechanisms and potential mobility. Ap Geochem 23:3545–3560. doi:10.1016/j.apgeochem.2008.08.014

Nurchi VM, Crisponi G, Villaesca I (2010) Chemical equilibria in wastewaters during toxic metal ion removal by agricultural biomass. Coord Chem Rev 254:2181–2192. doi:10.1016/j.ccr.2010.05.022

Ouellet S, Bussière B, Mbonimpa M, Benzaazoua M, Aubertin M (2006) Reactivity and mineralogical evolution of an underground mine sulphidic cemented paste backfill. Miner Eng 19:407–419. doi:10.1016/j.mineng.2005.10.006

Polat M, Guler E, Akar G, Mordogan H, Ipekoglu U, Cohen H (2002) Neutralization of acid mine drainage by Turkish lignitic fly ash: role of organic additives in the fixation of toxic elements. J Chem Technol Biotechnol 77:372–376. doi:10.1002/jctb.564

Potvin R (2009) Évaluation à différentes échelles de la performance de systèmes de traitement passif pour des effluents fortement contaminés par le drainage minier acide. PhD Diss, Chaire industrielle CRSNG Polytechnique—UQAT, Rouyn-Noranda, QC, Canada

Prasad PSR, Prasad S, Krishna V, Babu EVSSK, Sreedhar B, Ramana S (2006) In situ FTIR study on the dehydration of natural goethite. J Asian Earth Sci 27:503–511. doi:10.1016/j.jseaes.2005.05.005

Reynolds K, Petrik L (2005) The use of fly ash for the control and treatment of acid mine drainage. Proc, World of Coal Ash Symp (2005) Lexington. KY, USA

Seki K, Thullner M, Hanada J, Miyazaki T (2006) Moderate bioclogging leading to preferential flow paths in biobarriers. Gr Wat Monitor Remediat 26:68–76. doi:10.1111/j.1745-6592.2006.00086.x

Skousen JG, Ziemkiewicz PF (2005) Performance of 116 passive treatment systems for acid mine drainage. Proc, National Mtg of the American Soc of Mining and Reclamation, Lexington, KY, USA

Soleimani S, Van Geel P, Isgor B, Mostafa M (2009) Modeling of biological clogging in unsaturated porous media. J Contam Hydrol 106:39–50. doi:10.1016/j.jconhyd.2008.12.007

Twardowska I, Kyziol J (2008) Sorption of metals onto natural organic matter as a function of complexation and adsorbent-adsorbate contact mode. Environ Int 28:783–791. doi:10.1016/S0160-4120(02)00106-X

Vadapalli K, Klink M, Etchebers O, Petrik L, Gitari W, White R, Key D, Iwuoha E (2008) Neutralization of acid mine drainage using fly ash, and strength development of the resulting solid residues. S Afr J Sci 104:317–322

Van der Lee J (1993) JCHESS version 2.0. École des Mines de Paris, Centre d'information géologique, 2000–2001. http://chess.ensmp.fr. Accessed 15 Sept 2010

Zagury GJ, Colombano SM, Narasiah KS, Ballivy G (1997) Stabilisation de résidus acides miniers par des résidus alcalins d'usines de pâtes et papier. Environ Technol 18:959–973. doi:10(1080/09593330),1997,9618575

Zagury JG, Oudjehani K, Deschênes L (2004) Characterization and availability of cyanide in solid mine tailings from gold extraction plants. Sci Total Environ 320:211–224. doi:10.1016/j.scitotenv.2003.08.012